Molecular Crystals and Liquid Crystals Science and Technology. Section A. Molecular Crystals and Liquid Crystals

Publication details, including instructions for authors and subscription information:
http://www.tandfonline.com/loi/gmcl19

The Effect of Herringbone Order on the Nature of Smectic-A-Hexatic-B Transition in Thin Free-Standing Films of nmOBC

I. M. Jiang [a] & C. C. Huang [b]

[a] Department of Physics, National Sun Yat-sen University, Kaohsiung, Taiwan

[b] School of Physics and Astronomy. University of Minnesota, Minneapolis, Minnesota, 55455, U.S.A.

Version of record first published: 04 Oct 2006

To cite this article: I. M. Jiang & C. C. Huang (1997): The Effect of Herringbone Order on the Nature of Smectic-A-Hexatic-B Transition in Thin Free-Standing Films of nmOBC, Molecular Crystals and Liquid Crystals Science and Technology. Section A. Molecular Crystals and Liquid Crystals, 301:1, 385-390

To link to this article: http://dx.doi.org/10.1080/10587259708041792

Mol. Cryst. Liq. Cryst., 1997, Vol. 301, pp. 385-390
Reprints available directly from the publisher
Photocopying permitted by license only

THE EFFECT OF HERRINGBONE ORDER ON THE NATURE OF SMECTIC-A-HEXATIC-B TRANSITION IN THIN FREE-STANDING FILMS OF *nm*OBC

I. M. JIANG[1] AND C. C. HUANG[2]
[1]Department of Physics, National Sun Yat-sen University, Kaohsiung, Taiwan
[2]School of Physics and Astronomy, University of Minnesota, Minneapolis, Minnesota 55455, U.S.A.

Abstract Calorimetric, optical reflectivity, and electron-diffraction measurements have revealed several unique features near the smectic-A-hexatic-B transition of thin free-standing films of *nm*OBC (*n-alkyl*-4'-*n-alky*oxy-biphenyl-4-carboxylate). Our recent Monte-Carlo simulations of a coupled XY model offer important insight into the nature of this transition.

Soon after existence of the hexatic phase in the 2D system being theoretically proposed [1], the characteristic scattering pattern of this novel phase was discovered in one of the liquid-crystal mesophases found in *nm*OBC (*n-alkyl*-4'-*n-alky*oxy-biphenyl-4-carboxylate) [2]. Recently, employing heat capacity, optical reflectivity, and electron diffraction measurements [3-5] on thin free-standing films of 3(10)OBC, we have found the following *salient* features near the smectic-A (SmA)-hexatic-B (HexB) transition: 1) Unlike thicker films ($N > 2$), two-layer ($N = 2$) films display only a single heat-capacity anomaly, indicating that the two-layer films exhibit two-dimensional behavior. 2) To within the high resolution (about two parts in 10^5) of our measurement, the optical-reflectivity data display a smooth variation through the SmA-HexB transition with an inflection point located within 10 mK of the peak position of the heat-capacity anomaly. The optical reflectivity data are found to be continuous to within the 2 mK temperature resolution of this measurement [4]. These results indicate that the liquid-hexatic transition in 2-layer films is continuous. 3) Both heat-capacity and optical-reflectivity data can be well described by a power law expression with heat-capacity critical exponent $\alpha = 0.31 \pm 0.03$ [6]. According to the two-dimensional melting theory, the liquid-hexatic transition should belong to the XY universality class. Thus, these three experimental findings clearly indicate that hexatic order may not be the only order parameter responsible for the SmA-HexB transition in 3(10)OBC. Meanwhile, the existence of the herringbone order in this HexB phase has been clearly demonstrated by electron diffraction studies from an overexposed eight-layer 3(10)OBC film [5].

Being inspired by the above experimental findings, we have conducted computer simulations on the following coupled XY model [7] to gain further physical insight into the nature of this intriguing transition.

$$H = -J_1 \sum_{<i,j>} \cos(\psi_i - \psi_j) - J_2 \sum_{<i,j>} \cos(\phi_i - \phi_j) - J_3 \sum_{i} \cos(\psi_i - 3\phi_i) \qquad (1)$$

The first term describes the hexatic order ($\Psi = |\Psi| \exp(i6\psi)$) and the second one represents the herring bone order ($\Phi = |\Phi| \exp(i2\phi)$). Only the nearest-neighbor (<i,j>) coupling is considered. The coefficient J_3 determines the coupling strength between these two types of order (Ψ and Φ) at the same lattice site. We are interested in situations in which Ψ and Φ are coupled relatively strongly. Therefore, we choose $J_3 = 2.1$, $J_1 = 1.0$ and $0 < J_2 < 2.0$ for all of the work presented here.

The schematic phase diagram obtained from the Monte-Carlo simulations of heat capacity (C_v) on a 30 x 30 lattice is shown in Fig. 1 [6]. For sufficiently low values of J_2, the sequence of isotropic - hexatic - (hexatic & herringbone (denoted as H&H)) transitions can be identified. For example, Fig. 2 displays the simulation results for the case of $J_2 = 0.3$. The heat-capacity data exhibit a broad hump just above $T = 1.0$ which is followed by a sharp anomaly near $T = 0.43$. The hump manifests a defect-mediated 2D XY transition. The peak denotes a 3-state-Potts transition and is characterized by a heat-capacity critical exponent $\alpha = 0.36 \pm 0.05$ [6]. An interesting region of this parameter space is encountered for $J_2 > 0.75$ as the isotropic to H&H transition appears to be characterized by a single anomaly [6]. Detailed simulations yield continuous, sharp heat-capacity anomalies for $J_2 = 0.85$ and 0.95 which can be described by a power law with $\alpha = 0.36 \pm 0.05$ [6]. This is in reasonably good agreement with our 2-layer film results from five *nm*OBC compounds. Our simulations provide the same value of α for the hexatic-H&H and isotropic-H&H transitions, however, the helicity modulus results enable these transitions to be distinguished.

The unique properties of these two order parameters enables us to calculate the helicity modulus, an elegant concept introduced by Fisher, Barber, and Jasnow [8]. The helicity modulus is related to the difference in Helmholtz free energy obtained by applying periodic and twisted boundary conditions, namely,

$$F(\omega) - F(0) = 2\gamma(\beta)\omega^2. \qquad (2)$$

This expression represents a twist of phase angle ω applied along one axis of an N x N lattice. The coefficient $\gamma(\beta)$ is a measure of the rigidity of the system under an imposed

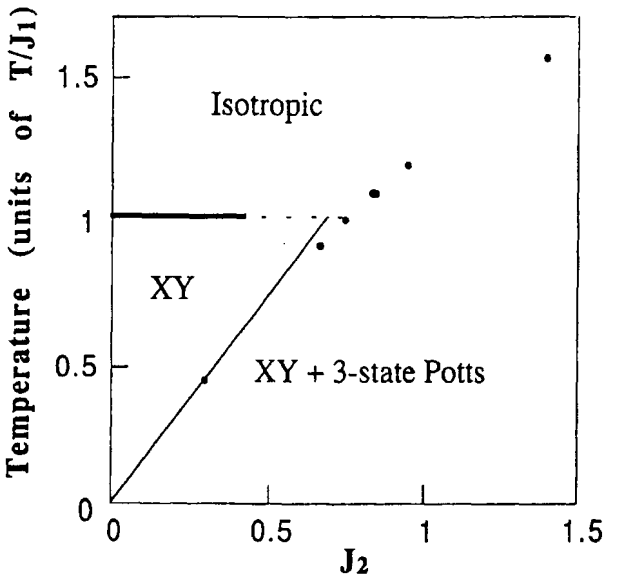

Fig. 1. Schematic of the phase diagram obtained from simulation results of C_v [6]: transition temperature versus J_2 with $J_1 = 1.0$ and $J_3 = 2.1$. The solid dots are determined by heat-capacity data. The narrow line is determined by the relationship $T_{c2} = 3J_2/2$ [10]. The heavy isotropic-XY transition line is assumed to be at T = 1.0. But as the temperature range for the XY state diminishes, it is very difficult to separate the small heat-capacity hump for the XY transition from the large heat-capacity peak associated with the three-state Potts transition. We have therefore used a dashed line in this region to indicate this uncertainty.

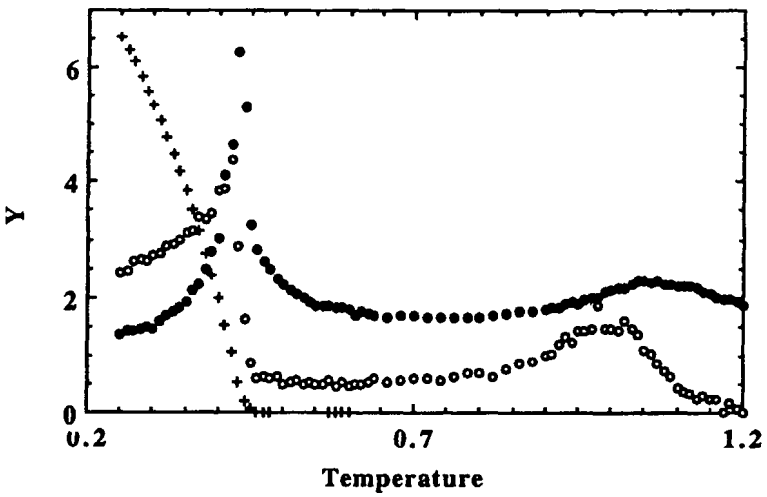

Fig. 2. Temperature dependence of the heat capacity (solid dots), the energy difference ($\Delta U/2$, open circles) and helicity modulus ($\gamma/2$, crosses) for $J_2 = 0.3$.

phase twist. On the basis of this definition, the difference between the internal energy obtained under periodic boundary conditions $\langle U_p \rangle$ and antiperiodic ($\omega = \pi$) boundary conditions $\langle U_a \rangle$ is related to the derivative of γ [8], namely,

$$(d[\beta\gamma(\beta)]/d\beta)\, \pi^2/2 = \langle U_a \rangle - \langle U_p \rangle = \Delta U. \quad (3)$$

To further investigate the nature of the single heat-capacity peak obtained in our simulations using J_2 =0.85 or 0.95, we have carried out helicity modulus calculations. Again, the work has been tested in an intuitively apparent region, i.e., $J_2 = 0.3$. The calculated internal energies acquired by applying periodic and antiperiodic boundary conditions provide both C_v and ΔU. The antiperiodic boundary conditions were imposed on both variables ψ and ϕ along one of the 2D lattice axes. The results after performing 500,000 Monte Carlo steps (MCS) are shown in Fig. 2. The heat-capacity data yield the expected result [6], a defect-mediated XY transition around $T = 1$ followed by a three-state-Potts transition near $T = 0.43$. The energy difference (ΔU) also provides distinct features associated with these two different phase transitions. $\Delta U = 0$ for a sufficiently high temperature, $T > 1.16$. Near the 2D XY transition, both C_v and ΔU yield broad humps with maxima located near $T = 1.07$ and 0.98, respectively. As expected, the peak position of ΔU more closely represents the reported defect-mediated transition temperature [9].

In the vicinity of the second transition, while C_v displays a fairly symmetric peak, ΔU exhibits a gradual increase followed by a sharp drop upon heating. The sharp drop in ΔU coincides with the heat-capacity peak position at $T = 0.43$. Between the two transitions, $0.46 < T < 0.6$, the ΔU remain fairly constant, reflecting the ψ order. After subtracting this residual difference, we can calculate γ for $T < 0.6$ due to the order of ϕ (see Fig. 2). As expected, in the vicinity of this transition, $\gamma \to 0$ as $T \to T_c^-$ and $\gamma = 0$ for $T > T_c$. The helicity modulus data shown in Fig. 2 could be fit to a simple power law expression, $\gamma = \gamma_0((T - T_c)/T_c)^{-\upsilon}$, yielding $\upsilon = 0.40 \pm 0.05$ and $T_c = 0.435$.

For $J_2 = 0.85$ or 0.95, the broad hump disappears. The C_v data display a symmetric anomaly. Figure 3 shows the results for J_2= 0.85. Again, ΔU remains zero in the disordered phase and exhibits a sharp rise in the immediate vicinity of the heat-capacity peak. No broad hump is discernible near $T = 1.0$ from either C_v or ΔU data. This strongly suggests a single transition from the isotropic to H&H phase. Non-zero values of ΔU just above the heat-capacity peak position appear to be due primarily to finite-size effects [10]. The helicity modulus obtained from ΔU can be fit to a simple power-law with critical exponent $\upsilon = 0.82 \pm 0.05$. These results indicate that both bond-orientational and herring bone order can be simultaneously created through a continuous transition characterized by a distinct helicity modulus critical exponent [10].

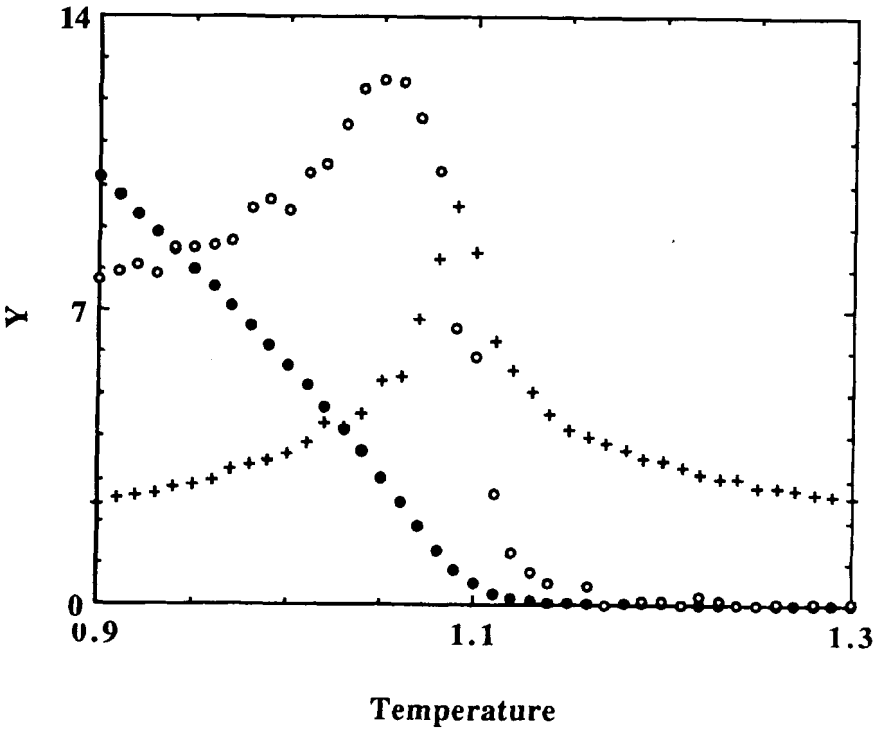

Fig. 3. Temperature variation of the heat capacity (crosses), energy difference ($\Delta U/2$, open circles) and helicity modulus (5γ, solid dots) for the case of $J_2 = 0.85$.

Employing finite-size scaling analysis to the sharp heat-capacity anomaly observed, we have obtained the heat-capacity critical exponent ($\alpha = 0.36 \pm 0.05$) which is in good agreement with the exponent ($\alpha = 1/3$) characterizing the three-state-Potts model in 2D [11]. However, the simple 3-state-Potts transition near $T = 0.43$ for $J_2 = 0.3$ is definitely different from the transition observed near $T = 1.09$ for $J_2 = 0.85$. The latter one establishes both herring bone and hexatic order. Although the distinction is not readily apparent based on heat-capacity critical exponents, the helicity modulus critical exponents are clearly different, indicating the uniqueness of this novel transition. In light of this simulation result, detailed analysis of the Hamiltonian (Eqn. 1) near the single phase transition region is essential to gain further physical insight into the nature of this novel transition. In a two-dimensional liquid helium film, the helicity modulus is related to the superfluid density. Hopefully, by obtaining better physical insight into the stacked hexatic

liquid-crystal phase found in *nm*OBC compounds, the calculated helicity modulus will be shown to be related to some measurable quantities.

The experimental determination of another critical exponent associated with the SmA-HexB transition of 2-layer *nm*OBC films would also provide great insight into the nature of this transition. However, to the best of our knowledge, no such critical exponent is readily accessible. Even though it is a very difficult task, in light of this simulation work, high-resolution experimental characterization of the range of the herring bone order in the hexatic-B phase of *nm*OBC becomes an important research project.

This work was supported by the National Science Foundation, Solid State Chemistry Program, Grants No. DMR 93-00781 and the National Science Council, Taiwan, Contract No. NSC 82-0208-M-110-072.

References

1. B. I. Halperin and D. R. Nelson, Phys. Rev. Lett. **41**, 121 (1978); A. P. Young, Phys. Rev. B **19**, 1855 (1979).
2. R. Pindak, D. E. Moncton, S. C. Davey, and J. W. Goodby, Phys. Rev. Lett. **46**, 1135 (1981).
3. T. Stoebe, C. C. Huang, and J. W. Goodby, Phys. Rev. Lett. **68**, 2944 (1992); T. Stoebe and C. C. Huang (unpublished).
4. T. Stoebe and C. C. Huang, Phys. Rev. E **49**, 5238 (1994).
5. T. Stoebe, J. T. Ho, and C. C. Huang, Int. J. Thermophys. **15**, 1189 (1994).
6. T. Stoebe, I. M. Jiang, S. N. Huang, A. J. Jin, and C. C. Huang, Physica A **205**, 108 (1994).
7. R. Bruinsma and G. Aeppli, Phys. Rev. Lett. **48**, 1625 (1982).
8. M. E. Fisher, M. N. Barber, D. Jasnow, Phys. Rev. A **8**, 1111 (1973).
9. R. Gupta, J. DeLapp, G. G. Batrouni, G. C. Fox, C. F. Baillie, and J. Apostolakis, Phys. Rev. Lett. **61**, 1996 (1988).
10. I. M. Jiang, T. Stoebe, and C. C. Huang, Phys. Rev. Lett. 76, 2910 (1996).
11. B. Nienhuis, A. N. Berker, E. K. Riedel, and M. Schick, Phys. Rev. Lett. **43**, 737 (1979).